SANDIA REPORT

SAND2013-8155
Unlimited Release
Printed September 2013

Theory and Modeling of Active Brazing

Frank B. van Swol, James E. Miller, Jeremy B. Lechman, Richard, C. Givler

Prepared by
Sandia National Laboratories
Albuquerque, New Mexico 87185 and Livermore, California 94550

Sandia National Laboratories is a multi-program laboratory managed and operated by Sandia Corporation, a wholly owned subsidiary of Lockheed Martin Corporation, for the U.S. Department of Energy's National Nuclear Security Administration under contract DE-AC04-94AL85000.

Sandia National Laboratories

Issued by Sandia National Laboratories, operated for the United States Department of Energy by Sandia Corporation.

Available to DOE and DOE contractors from
U.S. Department of Energy
Office of Scientific and Technical Information
P.O. Box 62
Oak Ridge, TN 37831

Telephone: (865) 576-8401
Facsimile: (865) 576-5728
E-Mail: reports@adonis.osti.gov
Online ordering: http://www.osti.gov/bridge

Available to the public from
U.S. Department of Commerce
National Technical Information Service
5285 Port Royal Rd
Springfield, VA 22161

Telephone: (800) 553-6847
Facsimile: (703) 605-6900
E-Mail: orders@ntis.fedworld.gov
Online ordering: http://www.ntis.gov/help/ordermethods.asp?loc=7-4-0#online

SAND2013-8155
Unlimited Release
Printed June 2013
Reprinted September 2013

Theory and Modeling of Active Brazing

Frank B. van Swol
Department 1814
Sandia National Laboratories
Albuquerque, NM 87185-1411
fbvansw@sandia.gov

James E. Miller
Department 1815
Sandia National Laboratories
Advanced Materials Laboratory
University Boulevard SE
Albuquerque, NM 87106
jemille@sandia.gov

Jeremy B. Lechman
Department 1516
Sandia National Laboratories
P.O. Box 5800
Albuquerque, NM 87185-0836
jblech@sandia.gov

Richard C. Givler
Department 1513
Sandia National Laboratories
P.O. Box 5800
Albuquerque, NM 87185-0836
rcgivle@sandia.gov

Abstract

Active brazes have been used for many years to produce bonds between metal and ceramic objects. By including a relatively small of a reactive additive to the braze one seeks to improve the wetting and spreading behavior of the braze. The additive modifies the substrate, either by a chemical surface reaction or possibly by alloying. By its nature, the joining process with active brazes is a complex nonequilibrium non-steady state process that couples chemical reaction, reactant and product diffusion to the rheology and wetting behavior of the braze. Most of the these subprocesses are taking place in the interfacial region, most are difficult to access by experiment. To improve the control over the brazing process, one requires a better understanding of the melting of the active braze, rate of the chemical reaction, reactant and product diffusion rates, nonequilibrium

composition-dependent surface tension as well as the viscosity. This report identifies ways in which modeling and theory can assist in improving our understanding.

Acknowledgment

Thanks to Allen Roach and Carlton Brooks for stimulating discussions of active brazes and surface tensions of metals. The ASC-PEM project is gratefully acknowledged for providing funding.

This page intentionally left blank.

Contents

Appendix

List of Figures

Preface

The process of active brazing is a highly complex one. It couples chemical surface reaction and interfacial diffusion to (surface)melting, surface roughness, wetting and spreading and flow. Given a typical braze, such as 97AG-1Cu-2Zr, and a ceramic substrate, such as alumina one seeks to produce a bond between braze and ceramic that hermetically seals and hence considerable mechanical strength and a lasting good performance. In the simplest instance a solid 'washer' of the active braze material is squeezed between the two ceramic surfaces. The assembly is put in an oven and subjected to a heating and cooling cycle to complete the bonding, while the oven atmosphere is controlled.

The brazing process presents a considerable challenge to efforts of quality control and reliability because it involves an intricate coupling of chemistry and physics taking place at an interface under high temperature conditions. Although surface chemistry and physics is a well-developed field in certain areas (e.g., certain gases or ordinary organic liquids) it is decidedly not for liquid metal mixtures. At present, very little is known about various important surface effects including surface segregation, surface melting, spreading and wetting. The lack of understanding is primarily due to the requirement of high-temperature and the opaqueness of liquid metals, which make experiments much more difficult.

It is natural to turn to molecular modeling and molecular theory to provide the much-needed insight to support the active brazing process. After all, the interface is of molecular dimension and high temperatures do not cause any problems when modeling. Also, liquid metal alloys (as opposed to molecular fluids, say) are so-called simple fluids, atomic fluids interacting through spherically symmetric potentials. This makes them good candidates for modeling with molecular level techniques such as molecular dynamics, Monte Carlo simulation, as well as mean field and classical fluid density functional theory. However, the mixture aspect does produce more of a challenge. In the bulk it can give rise to a complex phase diagram with many phases and possibly intermetallic compounds. At the interface it can enhance surface melting, and the (nonequilibrium) interfacial tension is expected to be sensitive to the local composition, potentially strongly affecting the wetting and spreading.

This document addresses several of the molecular phenomena that have been identified as potential role players in active brazing. In particular, we discuss surface chemistry, surface segregation and surface melting. We review the current understanding of the equilibrium metals (pure and mixtures) and discuss theory and techniques to model these. Finally, we visit the problem of diffusion in mixtures.

Summary

This report addresses various molecular scale phenomena important to the active brazing technique. In particular we discuss surface chemistry and surface melting. In addition, we review the status of molecular theory and modeling for both equilibrium metals and equilibrium alloys. Finally, we address diffusive transport in an equilibrium molten alloy. A complete description requires knowledge of the mutual diffusion coefficients as a function of composition. These quantities are difficult to measure, both in the lab and in the simulations. An approximate but comprehensive approach is outlined in this report and is based on the self-diffusion coefficient in mixtures, a quantity that is easy to calculate in simulations. In addition, we address the methods for calculating the viscosity. The report includes a chapter with recommendations that could be extremely helpful in providing a better understanding of the complex coupling of molecular processes that are involved in active brazing.

Nomenclature

brazing A metal-joining process whereby a filler metal is heated above melting point and distributed between two or more close-fitting parts by capillary action

active brazing brazing with a flller containing an active ingredient that can react and modify the surface to be joined

alloy a mixture ar solid solution of several metals.

liquidus a line in the temperature-composition diagram that separates an homogeneous liquid phase from a two-phase state of liquid plus solid

solidus a line in the temperature-composition diagram that separates an homogeneous solidphase from a two-phase state of liquid plus solid

Chapter 1

Introduction

In this report we address the metal joining technique of active brazing, a bonding process whereby a surface-active ingredient (i.e., Zr) is added to a metal alloy of silver and copper to promote better wetting and bonding between a metal and a ceramic (i.e., alumina) surface. The metal alloy will be put in contact with the ceramic surface and heated until the alloy starts to melt. The active ingredient will diffuse to the interface and be able to react with the ceramic, essentially replacing some Al atoms with Zr through the reaction

$$3\mathrm{Zr} + 2\mathrm{Al_2O_3} \rightleftharpoons 3\mathrm{ZrO_2} + 4\mathrm{Al} \tag{1.1}$$

The reduced Al ions will dissolve into the liquid metal alloy. Improved spreading is expected because the contact angle of Ag on ZrO_2 is smaller than that of Ag on Al_2O_3. The goal of active brazing at Sandia is to produce a metal-ceramic joint that is hermetically sealed, and of sufficient mechanical strength. Although this has been accomplished, in practice the process has at times been plagued by unexpected high failure rates, whose origin is not at all well-understood. To be able to systematically improve the process requires a better scientific understanding of the various sub-processes involved in active brazing: chemical reaction, diffusion, wetting, solidification, and their intricate coupling.

The history that led to the Ag/Cu/Zr braze formulation has been briefly reviewed[1].

In this report we will present a framework for predictive modeling of metal joining, and identify the various pieces that need to be addressed in order to accomplish this. Then we will outline, in detail, an approach that is firmly based in thermodynamics and statistical mechanics, that can provide the required thermodynamic and dynamic information.

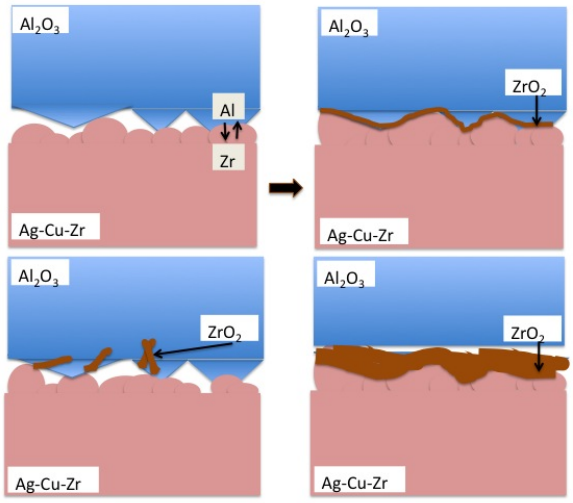

Figure 1.1. Schematic of the intended active brazing process. Top left panel: Alumina (blue, top) and a metal alloy (red,bottom) are brought into contact. Top right panel: upon heating in an oven to high temperatures, the metal alloy liquifies allowing Zr to react with the alumina phase. During the reaction Zr atoms replace Al atoms to form zirconia (brown). Ideally, the zirconia forms a very thin uniform layer at the interface that will promote wetting and spreading of the molten alloy, leading to strong and sealing bond between the metal and ceramic phases . The bottom row illustrates two types of *unsuccessful* brazing joints. If Zr reacts unevenly with the alumina phase the resulting zirconia will not constitute a thin uniform layer but rather produce uneven regions. As a result, the wetting and spreading of the liquified alloy will be uneven, and the final joint may exhibit voids (bottom left). If the extent of reaction is too large, the zirconia layer may end up to thick (bottom right). The lattice mismatch between zirconia and alumina may then lead to cracks or delamination, also resulting in bad seals and weak bonds.

Chapter 2

Interfacial Phenomena

Interfacial chemistry

The mechanism of the active brazing is a reaction or interaction at the interface which forms a layer that is better wetting by the filler metal, observable for example in the laboratory by a reduction in the contact angle (c.f., work of adhesion) as the interfacial reaction proceeds[2]. In the case of the Ag/Cu/Zr braze, Zr is presumed to react with Al_2O_3 to form ZrO_2. The Cu is present to change the flow characteristics and prevent so-called runout. One would begin with the assumption that a homogeneous thin layer of uniform thickness of ZrO_2 on Al_2O_3 is the preferred geometry (see figure 1.1), as the intermolecular forces that determine the wetting behavior are known to be of short-range, of the order of a nanometer. Note however, that this may not be true, oxide "fingers" growing into alumina layers of thermal barriers have been known to improve adhesion (for instance, limit spallation)[3].

The reaction of Zr with Al_2O_3 (to form Al and ZrO_2), equation 1.1, is mildly thermodynamically unfavorable at temperatures below ca. 675 °C which corresponds roughly to the melting point of Al: 660 °C[1], and only mildly favorable above this point (see figure 2.1). In contrast, the reaction of Zr with SiO_2 ($Zr + SiO_2 \rightleftharpoons Si + ZrO_2$) is calculated to be significantly more favorable throughout the temperature range of interest (i.e., ΔG <-40 kcal/mol), as is the reaction of Zr with Si to form silicides. The ΔG calculated for the reaction to form Zr_5Si_3, the only zirconium silicide in the HSC database[4] is <-135 kcal/mol. Many other silicides are known and are reported to have high heats of formation and can be synthesized straightforwardly for example by ball milling mixtures of Zr and Si (see reference [31]). Likewise, Zr thin films are reported to react with SiO_2 at temperatures as low as 650°C to form silicides at the interface with an overlayer of ZrO_2[32]. Therefore, from a thermodynamic standpoint the Zr would prefer to react with SiO_2 rather than Al_2O_3; likewise the reaction of Al with SiO_2 to form Al_2O_3 and Si is also favored. This reaction has in fact been observed at Al/SiO_2 interfaces, e.g., such as might be present in integrated circuits[33]. Cu will not reduce Al_2O_3 or SiO_2. Copper is maintained at a low concentration ($\leq$ 2%) as it has been observed that Cu forms the Cu_4AgZr phase at higher concentrations causing poor performance[1],[34],[35]. Al can also form precipitates with Cu[35].

To summarize, thermodynamics predicts that the equilibrium in a Zr/Al_2O_3/SiO_2 system would favor oxidation of Zr to ZrO_2 via reduction of SiO_2 to Si, and possibly the subsequent reaction to

[1] note that this is significantly less than the melting temperatures of Ag, 962 °C, or Cu, 1085 °C

form silicides, preferentially to the reduction of Al_2O_3 to Al. Cu is presumably uniformly distributed and unreactive provided the concentration is low (however, see the section on surface segregation and surface melting below). Note that the thermodynamic effects of the predominantly Ag phase (e.g. possible solution phases), or reaction at the metal/Ag interface are not considered here. The thermodynamics and phase equilibrium of the Ag/Zr/Cu system has recently been reviewed by Kang and Jung[36].

The utility of thermodynamics outlined here is limited to realm of equilibrium (i.e. long reaction times). The reactions that are observed and the extent of these reactions is subject to additional considerations such as diffusion and reaction rates (which in turn are subject to temperature), time scales, as well as to stoichiometric considerations (i.e. the amount of filler material and hence Zr available, the composition and the ceramic surface, etc.) and potentially to other parameters such as the initial state of the system (impurities such as oxides, homogeneity of the oxide surface, etc.). The uniformity of the reaction is subject to similar considerations.

The extent of reaction is relevant as some controlled laboratory studies of the reaction of Ag/Zr with Al_2O_3 ($> 99\%$ purity) have shown evidence of significant variations in the zirconia/alumina interface, including for example detachment of the zirconia (i.e., a Ag rich layer between the Al_2O_3 and ZrO_2) and columnar growth of ZrO_2 with a interpenetrating Ag-rich phase. Deep penetration into the alumina has also been observed as the reaction proceeds (see Loehman et al. [37],[38]). These effects have not definitively been tied to reaction extent, e.g., layer thickness or particle size, alone; reaction temperature may also be driving these effects as the temperature was elevated to 1160°C to speed the progress of the reaction. Additionally, we note that these results may not be indicative of the actual system due to the high purity of the alumina substrates. Results for zirconia barrier layers on alumina have shown that the structure and quality of the barrier layer is dependent on whether 96% or 99.5% alumina is used and, to some extent, on the thickness of the layer. The less pure substrate led to more uniform layers[39]. Additionally, note that as the reaction proceeds, ever more Al (or Si) is liberated, which may have unintended consequences (good or bad). The relative amounts of Zr (total, not concentration) available in these experiments versus the system of interest is not currently known.

Nonetheless, these results raise question as to the integrity of the zirconia/alumina interface. In this regard we note that calculations indicate that the zirconia/alumina bond is relatively weak[40], [3]. Further, we note that zirconia has monoclinic, tetragonal, and cubic crystal forms. For bulk samples, zirconia is monoclinic at room temperature, while the tetragonal phase is stable at temperatures above 1170°C. However, the transition is observed to be spread over a broad temperature range (e.g. 930 -1260°C)[41]. The transition from the tetragonal phase to the monoclinic phase results in a volume increase of $>4\%$. Therefore, zirconia is typically doped with other elements (e.g., Y, Ca, Mg, etc.) to stabilize the material in part or in full to avoid mechanical issues and breakage that could result from this behavior. For example, microcrack formation at the interfaces of zirconia and alumina in composite fibers has been attributed to the combined effects of this phase change and difference in thermal expansion[42]. Alumina has been reported as a dopant with high solubility that stabilizes the tetragonal phase of zirconia[43]. Conversely the presence of silica has been reported to destabilize the tetragonal thin films of yttria-stabilized (3 mol%) zirconia on alumina[39]. To further complicate the issue, the phase stability is a function of size

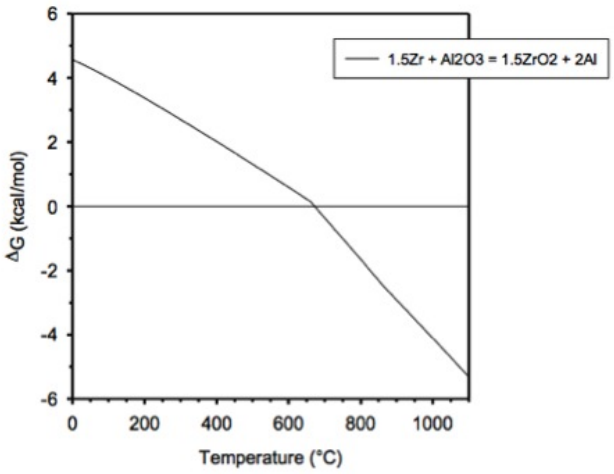

Figure 2.1. Gibbs free energy change for the reaction of Zr with aluminum oxide as calculated using HSC chemistry v. 7.11 see reference [4].

for particles $<$ ca. 100 nm[44], and possibly of particle shape[45]. The transition temperature is pushed to lower temperatures as the size is decreased, so that the tetragonal phase is stable at room temperature for very small particles. As one might anticipate, the presence of dopants alters the size dependent transition temperature[46]. The only document we have seen to date that identifies the zirconia phase resulting from the reaction of Ag/Zr with alumina reports it as monoclinic (see Loehman et al.[38]).

Wetting and spreading

A liquid metal spreading on a metal surface introduces additional complexities into the description of the moving fluid-solid interfacial boundary. Primary amongst these are the effects of mixing, preferential adsorption and dissolution processes that are common at the solid-fluid interface. That is, metal atoms of the rigid solid may leave the solid and dissolve into the liquid metal. Simultaneously, metal atoms in the liquid may leave the liquid and be integrated into the solid boundary. These two mixing processes will affect the local composition of the liquid as well as the solid. In adsorption processes, inhomogeneous composition throughout the interface may develop

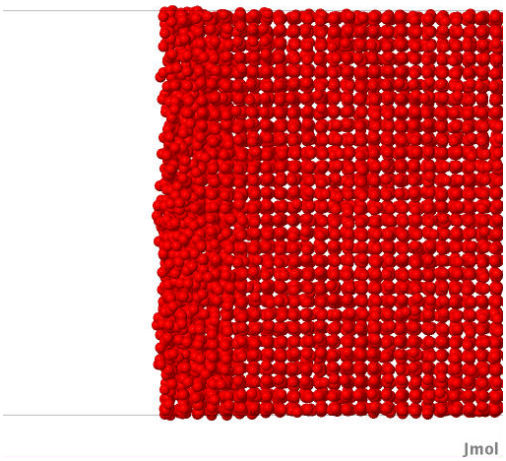

Figure 2.2. Snapshot of a solid-vapor Pt interface, just below the the bulk melting temperature. We show the left-hand side of a slab of Pt, with a (100) surface (simulated with an EAM potential). The snapshot illustrates surface melting of the Pt solid: about 5 to 6 of the outermost layers have undergone melting. The thin layer of liquid at the solid-vapor interface constitutes an equilibrium state.

as one species of the liquid exhibits preferential adsorption at the solid-liquid interface.

No matter what the underlying causes, composition changes of the liquid and solid phases will produce a change in the liquid-solid interfacial free energy ("surface tension"[2]) as well as possibly in the transport properties (i.e., the viscosity). Changes in the surface tension imply a variation in the contact angle, which will influence the movement of the contact line. Thus, formally, the contact angle, θ, is to be considered a function of the interfacial composition, which itself is a function of time.

Surface melting: pure metals

Surface melting is a form of premelting (melting below the bulk melting temperature) that can occur at the interface between a solid and a vapor phase. More generally, interfacial melting can occur when a solid meets another phase, for instance another solid (e.g., alloy and ceramic), or even when two grains meet at a grain boundary. Surface melting occurs when the interfacial tensions are such that the surface free energy is lowered by premelting of the solid phase (i.e., the alloy phase), producing a thin liquid layer at the solid-solid interface. The liquid layer thickness grows

[2]Strictly, a surface free energy per unit area. For liquid-vapor interfaces the surface free energy is always positive, thus justifying the term "tension". However, at a solid boundary the surface free energy can be of either sign. In practice, the sign does not affect the convention to use the term surface tension for all interfaces.

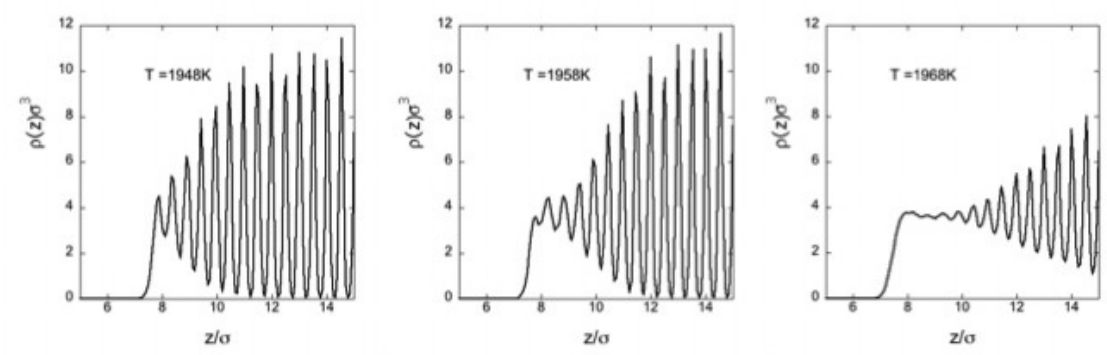

Figure 2.3. Density profiles for the left-hand side of an fcc platinum slab with (100) surface centered at $z/\sigma \approx 18$ for different temperatures (σ = 0.392 nm represents the T=0 K lattice constant). The number of liquid layers increases from left to right as the bulk melting temperature is approached.

as the temperature approaches the bulk melting temperature from below. This is a well-known phenomenon at the pure solid-vapor interface, and it is known that premelting depends on crystal orientation. Premelting is possibly more pronounced when the solid is not pure but rather an alloy phase. For an alloy (and away from any eutectic) even the bulk melting already takes place over a range of temperatures, while the compositions of bulk solid and bulk liquid vary. It is quite likely that the premelting of an alloy will be more pronounced and quite sensitive to the concentration and distribution of the minority elements (Cu and Zr). Once the interfacial zone premelts, the Zr can diffuse rapidly and the interfacial reaction can proceed. In turn,the reaction product, Al, will initially be limited to the thin premelted layer. The changing composition of the premelted layer may lead to enhanced or possibly reduced premelting. Nothing is known about alloy interfacial premelting at the present time. However, it is obvious that if premelting of the alloy takes place that both the wetting properties and the extent of reaction will be sensitive functions of the local temperature and time of the active brazing process.

The surface reconstruction that was observed prior to melting of the crystallites can perhaps be viewed as a manifestation of surface melting, a surface phase transition whereby a thin liquid layer is produced, intruding between the bulk crystal and the bulk vapor. At the surface melting transition the free energy of prematurely converting a number of crystal layers into liquid is balanced by the reduction in total surface free energy that results from replacing the single crystal-vapor interface by two interfaces, the crystal-liquid and liquid-vapor interfaces. Surface melting can (but does not necessarily) occur for certain solids and specific crystallographic directions. We studied the behavior of the three most close-packed surfaces of fcc platinum, the (111), (110) and (100) surfaces, by generating a thick slab of an fcc crystal. In each case the temperature was increased in small steps, while the lateral (periodic) dimensions were expanded according to the volume expansion with temperature at zero pressure that we determined in a bulk study. The results are summarized

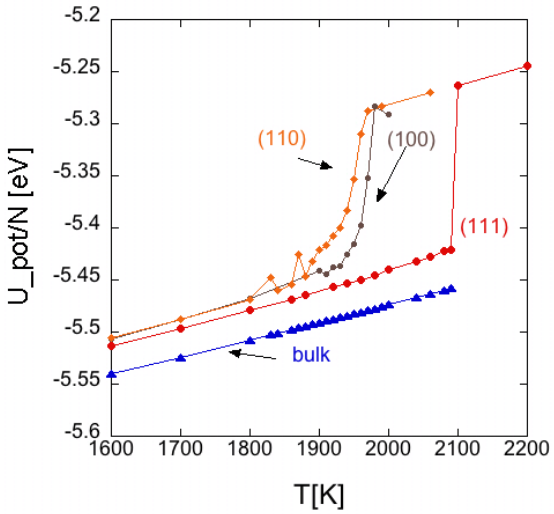

Figure 2.4. Potential energy per particle versus temperature for bulk fcc platinum (blue) and thick slabs of platinum with (111), (110), and (100) surfaces

in Fig 2.4, where we plot the potential energy per particle as a function of temperature. The bulk curve (no surfaces) is shown for comparison. The increase of the potential energy per particle for the slabs is entirely due to the surface energy contribution. We note that the surface free energy of the (100) and (110) surfaces is indistinguishable below the melting temperature, but noticeably larger than the (111) surface energy. A precise determination shows that the difference is about 1 eV/nm2.

To investigate the surface phenomena in more detail consider the curve for a crystal slab with two (100) surfaces. As the temperature reaches about 1950 K the potential energy starts to climb to about -5.398 eV per particle. At this point the system has surface-melted 4-5 layers on each side of the slab as can be seen from the density profiles perpendicular to the interface that are shown in Figure 2.3. Here, for clarity, we show only the interfacial region of the profile on the left hand side of the slab. The center of the slab is roughly at z/σ = 18, and the other interface is located at approximately z/σ = 30 (here σ equals 0.392 nm and is an accurate measure of the diameter of a Pt atom). Over a range of approximately 20K (which corresponds to about 1% of the melting temperature) we see first that the $\sim$ 2-4 outer layers start to merge and exchange atoms (as evidenced by a non-zero local density between peaks). As the temperature increases (bottom panel), these layers become liquid. The surface disordered state is an equilibrium state for which the center of the slab remains crystalline while the surface consists of a thin fluid layer. As the temperature is increased the thickness of the fluid layers grows. This is in accordance with general predictions for surface melting (see reviews). For short-range forces, such as we have here, the thermodynamic approach predicts the liquid layer thickness $d \sim ln|t|$, and for long-range forces $d \sim t^{-1/3}$, where t denotes the reduced temperature $(T_m - T)/T_m$.

Alloy surfaces

Given that the underlying argument for surface melting, a trade-off between the free energy cost of premature melting and the reduction in interfacial free energy, is a general thermodynamic one, it follows that alloys are expected to exhibit surface melting as well. However, the multi-component aspect makes alloy surface melting a richer phenomenon, since there is surface segregation and bulk alloys generally melt over a range of temperatures while continuously changing the composition of both the melt and the solid.

The active braze of interest is a silver-copper-zirconium alloy with 97w% Ag, 1w% Cu, and 2w% Zr (known as "97Ag-1Cu-2Zr") or, more helpfully, in atomic percentages: 96% Ag, 1.7% Cu, and 2.3% Zr. Typically alloys are expected to show surface segregation. That is, the concentration of the components at the surfaces is not equal to that in the bulk. Thus, the concentration of Cu and/or Zr at the surface is expected to be different from that in the bulk. This is similar to what is found in liquid mixtures. The surface concentration can either be higher (positive adsorption) or lower (negative adsorption), depending on the surface free energy.

Surface segregation

Insight into the segregation behavior in a crystal can be obtained from the segregation energy at infinite dilution. The segregation energy of an impurity of species α placed in crystal layer i from the surface inside a host crystal of species β is defined as

$$E_i^{\alpha\beta} \equiv U_i^{\alpha\beta} - U_\infty^{\alpha\beta} \tag{2.1}$$

where $U_i^{\alpha\beta}$ is the potential energy of the impurity in layer i, and $U_\infty^{\alpha\beta}$ is the potential energy of the impurity in a bulk layer.

Zhang et al. [5] have performed a modeling study (at $T = 0$K) to determine the segregation energies of a large number of metal impurities in various fcc metals (including Ag and Cu, but not Zr), focusing on the (100) surface. They considered the four outermost layers, i.e., $i = 1$ to 4, and observed that the magnitude of $E_1^{\alpha\beta}$ exceeds that of the next three layers, and futher $E_i^{\alpha\beta} \approx 0$ for $i > 3$. The magnitude of $E_i^{\alpha\beta}$ decays either monotonically or in oscillatory fashion. Thus the largest effect of an impurity comes from the outermost layer. The authors report that $E_1^{\alpha\beta}$ can be positive or negative. The sign of $E_1^{\alpha\beta}$ correlates strongly with the difference in surface free energy, U_s^α - U_s^β, of the (100) surface of the pure metals involved (i.e., the pure metals of species α and β). That is, a positive segregation surface energy of impurity α in host β results when U_s^α - $U_s^\beta > 0$, and vice versa. Thus, the impurity with the lower surface energy will segregate to (i.e be positively adsorbed at) the surface of the host with the larger surface energy[3].

From Zhang et al. [5] we observe that $E_1^{Cu\,Ag} = 0.1613\ eV > 0$, indicating that Cu will be negatively adsorbed onto the solid-vapor interface. Unfortunately, the authors do not supply any information regarding Zr.

Surface melting

As the bulk alloy is heated and the temperature increases it will eventually exhibit melting. Before we discuss surface melting, we briefly review the bulk melting process. In contrast to the melting of a pure metal, the melting of an alloy takes place over a range of temperatures that start when the solidus temperature is reached, and is complete when the liquidus/indexliquidus temperature is reached. During the melting process, the composition of the liquid metal alloy mixture is typically *not* equal to that of the solid phase alloy with which it is in equilibrium[4]. Typically, for nearly pure alloys, such as the active braze considered here (i.e., 97Ag-1Cu-2Zr), the solidus and liquidus temperatures are below that of the pure host melting temperature, and the

[3]This is analogous to the behavior of liquid mixtures, where one observes that the most volatile component is positively adsorbed at the liquid-vapor interface.

[4]The familiar but still rare exception is that of the eutectic alloy, for which the melting range is reduced to a point, and thus the liquid composition equals that of the solid.

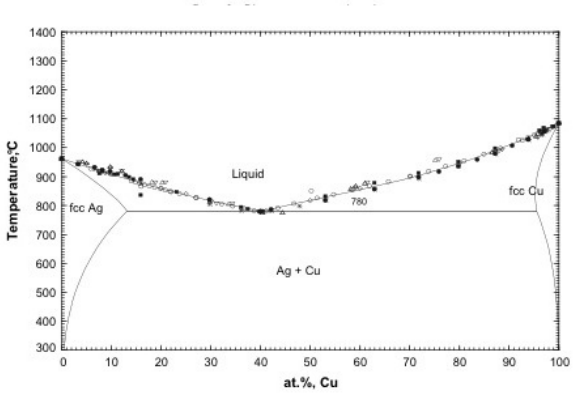

Figure 2.5. The phase diagram of the binary Ag-Cu alloy. Reproduced from reference[36]. This alloy exhibits a eutectic at approximately 40% Cu.

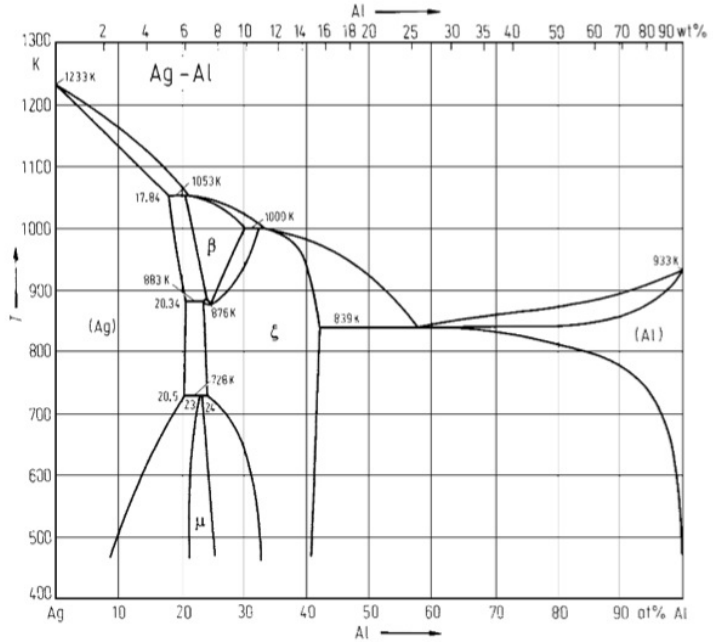

Figure 2.6. The calculated phase diagram of the binary Ag-Al alloy (see ref [49]).

liquid phase is richer in the "impurities" than the the solid phase. To illustrate, in figure 2.5 we reproduce the phase diagram of the binary alloy Ag/Cu.

The alloy melting process is illustrated in detail in figure 2.5, which shows a sketch of a simplified phase diagram. At the solidus temperature, when the liquid first appears, the liquid phase is the most rich in impurities(see figure 2.7). Conservation of mass dictates that as the temperature is raised further both coexisting liquid and coexisting solid gradually becomes less rich in impurities. Eventually, when the liquidus temperature is reached the melt has the same composition as the initial solid alloy. This part of the alloy melting process is analogous to the distillation process of liquid mixtures, and we note that both the surface segregation and the alloy melting phenomena are being exploited for metal purification and collection of trace elements.

Now consider the surface region where, as we have seen above, segregation effects can imply an impurity molefraction x_s that differs from the bulk molefraction, x_b. The case of positive adsorption, $x_s > x_b$, is sketched in figure 2.7. To facilitate the discussion, we consider the surface region as a distinct "phase"[5]. When the system is heated the impurity-enriched surface phase will reach the solidus line at a temperature that is *below* that of the bulk phase. This stems from the fact that the solidus in figure 2.7 has a negative slope with increasing molefraction. We note that this case is representative of the most relevant region of the actual Ag/Cu phase diagram of figure 2.5, namely the region of small impurity molefractions. From that figure we estimate that the solidus slope implies a reduction of approximately 11°C reduction for every percent increase in the impurity (i.e., Cu). We stress that although this argument leads to pre-melting of the surface phase it is to be distinguished from the surface melting described earlier. That is, the temperature effect considered here *not* driven by interfacial free energy lowering that is the defining characteristic of surface melting. Rather, the melting of the surface at hand stems entirely from the impurity enrichment , which in our example happens to be located at the surface.

We can readily modify the case described above and change the impurity surface segregation from positive to negative adsorption. This implies that now we have $x_s < x_b$, placing x_s to the left of x_b in figure 2.7. This indicates that the surface melts at a higher temperature than the bulk. A eutectic alloy is a special case. The bulk will melt completely at a unique temperature. Surface segregation of either kind (i.e., positive or negative) will lead to a situation where the surface will melt at a higher temperature than the bulk, since the solidus slopes upwards on either side of the eutectic.

The enrichment induced melting just described and the traditional surface melting phenomena can lead to an interesting interplay in alloys. Generally speaking, one can expect situations where only one of the two phenomena occurs, as well as where both are at work. In the latter situation the synergy can be positive or negative. In the absence of segregation, only interfacial tensions could produce melting of the surface. On the other hand, a (111) surface of Ag, say, which does not surface melt in the pure state, can only exhibit melting at the surface if there is impurity segregation.

Their does not appear to be any experimental studies in the literature that have addressed sur-

[5]The argument developed here also applies, without change, to a bulk phase of an alloy that has a heterogenous composition, i.e., regions of high and low impurity molefractions.

face melting in alloys. But we identified one theoretical study that addresses the phenomenon. An interesting mean field lattice gas study of surface melting of alloys was performed in 1999 by Teraoka and Komaki[47], building on Teraoka's earlier studies of surface melting of pure systems[48]. Teraoka is able to use the lattice gas model to represent a solid by modifying the traditional lattice site by subdividing a site into three states. The lattice gas Hamiltonian then specifies different coupling constants for interactions between the different states of two neighboring occupied sites[6]. Although the mean field lattice gas is a fairly crude model of a solid-liquid-vapor system, it is able to represent the basic physics of alloys. In particular, the model is sophisticated enough to capture the interplay between compositions (such as phase diagrams) and interfacial phenomena (such as surface melting). The free energy minimization used by Teraoka and Komaki[47], and performed to determine equilibrium profiles, essentially constitutes a density functional theory of their lattice gas model.

Clearly, molecular simulation (molecular dynamics or Monte Carlo) is an ideal technique to study the variety of cases of anticipated surface melting in alloys, since it is straightforward to introduce impurities and to vary their nature by simply modifying their potential parameters at will.

Turning now to surface melting of alloys, we anticipate that there is likely a relationship between surface segregation and surface melting. For instance, in the case of positive adsorption (for instance the 99Ag-1Cu alloy) the impurity concentration is larger in the surface region. The bulk phase diagram would then suggest that the solidus of the surface region is below that of the bulk region, promoting surface melting.

Solidification

During (or following) the spreading or infiltration by the liquid metal, parts of the liquid will reach a condition that is either a glassy state, or a state point beyond a phase boundary, where the current, cooled, liquid phase becomes unstable with respect to phase separation, or unstable with respect to crystallization (or both). A phase transformation heralds an abrupt change of certain materials properties. For instance, crystallization will cause an enormous increase in some properties, i.e., the viscosity (a near divergence), an enormous decrease in others such as the diffusivity. Other properties will undergo step changes (e.g., density, heat capacity).

Crystallization proceeds by nucleation and growth, and depending on how rapidly the cooling takes place, and depending on the composition as well as the nonuniformity of composition, the system will typically end up displaying many crystalline domains or grains, meeting at grain boundaries.

If the system manages to avoid crystallization then the atom's dynamics will be arrested in a more gradual way. This can be the likely result of compositional effects. Two metals A and B may be miscible in the liquid phase over a large range of composition, but at low temperature the equilibrium crystal may be of a distinct stoichiometric composition, such as AB_2. A liquid sample

[6]Teraoka's model would appear to be very similar to a four-state Potts model.

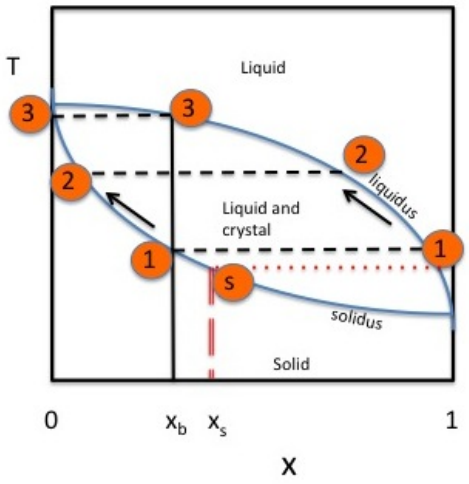

Figure 2.7. Simplified schematic phase diagram of a binary alloy illustrating the compositional changes that take place as the temperature of an initially entirely crystalline solid alloy of bulk composition x_b is increased. The abscissa denotes the molefraction of the "impurity". Bulk melting first happens when the alloy temperature reaches the solidus line at the point marked "1" (on the left). The location of the liquidus line determines the molefraction of the first alloy liquid phase. The latter is defined as the intersection of the horizontal dashed line and the liquidus curve (a point also marked "1", located at a molefraction considerably larger than that of the original solid (x_b)). As the temperature is further increased more of the solid phase melts. As this happens, the composition of the coexisting phases changes (indicated by the symbol "2"), both move to left in the diagram. That implies that as the temperature is increased the composition of *both* coexisting phases becomes more dilute in the impurity. Melting is completed as the liquidus curve is reached, and the last amount of solid disappears. The final amount of solid has a composition marked "3" (on the left) and represents the maximum purification of the solid that can be accomplished when given an alloy at composition x_b. Obviously, the final liquid phase must possess a composition equal to that of the starting solid (i.e. x_b). The melting of a segregated surface "phase" is also indicated in the figure (vertical red line, long dashes). For a surface that exhibits positive adsorption of the impurity, the surface impurity molefraction, x_s, will lie to the right of x_b. Consequently, the surface phase will reach the solidus at a lower temperature than does the bulk. This point is marked "*s*" in the figure.

of initially equal amounts of A and B will need to phase separate as well to grow into a AB_2 crystal. If the mutual diffusion coefficients of A and B atoms is sufficiently slow (for a given cooling rate) then the fluid may not be able to nucleate and grow the AB_2 phase. Instead, the result would be a glassy phase of equal amounts of atoms A and atoms B. Alternatively, small crystalline regions of AB_2 may from but end up coexisting with a A-rich glassy phase.

This part of the metal joining process concerns the phase transformation in metal mixtures from the liquid phase. The ultimate kind of microstructure that results is a well-studied area, and previous research has revealed that the microstructure is a strong determinant of the future materials behavior of the metal joint. In conclusion, solidification of the metal joint can, for the purposes of this paper, be considered an essentially understood phenomenon that can be treated with existing strategies.

The important conclusion is that the spatial composition variation of the fluid phase (as it results from the reactive wetting process) serves as the initial state for the solidification. Hence, a sufficient understanding of the wetting process may have an important role to play in determining a desirable final microstructure of the metal joint.

For instance, consider manufacturing a metal joint through an infiltration process. The surface reaction will produce atoms B whose spatial distribution is nonuniform, as different parts of the infiltrating liquid have experienced different residence times inside the pore. Near the meniscus we expect to see more uniformity and a higher concentration, whereas near the entrance (on the reservoir side), we expect smaller concentrations of B and less uniformity.

A predictive modeling capability would enable one to explore the *inverse optimization* problem: what initial composition distribution(s) of the infiltrating liquid at the entrance would produce a final joint after infiltration that is most uniform (and thus most desirable)? This could be powerful as it enables fine control over the final properties of a metal joint.

This page intentionally left blank.

Chapter 3

Equilibrium Pure Liquid Metals

Equilibrium pure liquid metals.

The fact that for the problem at hand liquid metals can be considered classical simple liquids helps to make the problem considerably more tractable. That is, liquid metals are atomic fluids, and can be successfully described with with interatomic potentials that are spherically symmetric and short-ranged. The classical potential of choice is the embedded-atom method (EAM) potential, which is a multi-body potential with a contribution that depends on the local density surrounding two interacting atoms i and j. However, the potential energy EAM potential can still be written as a function of all the pair distances. As with traditional pair-potentials, the force of a particle i, $\mathbf{F}_i$, can still be written as a sum over central pair forces, $\mathbf{F}_{ij} = -\mathbf{F}_{ji}$, i.e.,

$$\mathbf{F}_i = \sum_{j \neq i} \mathbf{F}_{ij}. \tag{3.1}$$

Molecular simulation

As a result of the pair property for the energy, it is straightforward to perform standard molecular simulations (molecular dynamics or Monte Carlo) for metals; and a definition of a local pressure tensor (the negative of the Cauchy tensor) is free of complications, as is the mechanical route to the surface tension.

Perturbation theory

In addition, just like the quintessential simple liquids, the noble gases, the liquid structure of metals is dominated by the short-range (repulsive) part of the interatomic potential. Loosely speaking, a liquid metal can be considered to be a collection of repulsive spheres moving around in a more uniform attractive background. As a result, one can successfully apply WCA (Weeks, Chandler and Andersen) perturbation theory, which starts by writing the interatomic potential as the sum of a repulsive and an attractive term. The repulsive term is so short-ranged that it can be represented by a hard sphere potential (with a suitable hard sphere diameter). Hence the liquid

structure, as expressed by the radial pair distribution function, $g(r)$, and thus all the equilibrium thermodynamic properties can be calculated from the knowledge of the free energy of the hard sphere fluid and the application of an attractive perturbation. The attractive contribution is calculated as an integral over the reference fluid's $g(r)$. This produces very accurate thermodynamic properties of the dense fluid, typically within $1-2\%$ of the values calculated by the 'exact' molecular simulation approach. In a strict mean field theory a further approximation is made: $g(r) \approx 1$. This, of course, simplifies the calculation at the expense of reduced accuracy of the equation of state.

Classical Fluids DFT

The strict mean field equation of state is what underlies classical fluids density functional theory (CF-DFT). This is an important observation since CF-DFT can be viewed the inhomogeneous analogue of perturbation theory and strict mean field theory. It is a powerful technique that allows one to determine the interfacial properties, that is, density and composition profiles and the surface free energy.

Dynamical Properties of liquid metals

Over the decades there has been much effort devoted to predicting the self-diffusivities of simple liquids. The basic assumption (see the work of Protopapas, Andersen and Parlee [12]) made is that the self-diffusion coefficient of a simple liquid is equal to that of an appropriate hard sphere(HS) fluid. The basic idea for this assumption, contrasting the roles of repulsive and attractive forces, goes back to van der Waals and Boltzmann (see the paper by Ben-Amotz and Herschbach [19]) and it has been embodied in modern theory of fluids . Since the hard sphere fluid is characterized by just the hard sphere diameter, determining the appropriate hard sphere fluid is equated with specifying a hard sphere diameter for the simple ilquid of interest.

Thus, two ingredients are required, 1) the sefl-diffusivity of the hard sphere fluid as a function of density, 2) a determination of the equivalent hard sphere diameter.

Hard sphere self-diffusivity. Enskog Theory.

The well-known Enskog theory approximation for the hard sphere self-diffusion coefficient is

$$D_E = \frac{3}{8\rho\sigma^2}\left(\frac{kT}{\pi m}\right)^{1/2}\frac{1}{g(\sigma)} \equiv \frac{D_0}{g(\sigma)} \tag{3.2}$$

where m and σ denote the mass and diameter of the hard sphere, k is Boltzmann's constant and T is the absolute temperature, and ρ is the number density. $g(\sigma)$ is the value of the radial distribution

function , $g(r)$ (or rdf), at contact (i.e., at closest approach: $r = \sigma$). The latter is related to the equation of state. In terms of $Z \equiv p/kT$ (the compressibility factor), we have

$$g(\sigma) = \frac{Z-1}{4\eta} \approx \frac{1-\frac{1}{2}\eta}{(1-\eta)^3} \tag{3.3}$$

where the packing fraction $\eta = (\pi/6)\rho\sigma^3$ characterizes the dimensionless density.

At low densities $\eta < 0.1$ the Enskog expression is accurate. At intermediate $\eta \leq 0.4$ it is too small, while for larger values, it rapidly becomes too large. Using MD HS data a better fit has been developed for the HS self-diffusivity (D_{HS}) which covers the entire density range, all the way to random close packing:

$$\begin{aligned} D_{HS}(\eta) &= D_E(\eta) f_D(\eta) & (3.4)\\ f_D(\eta) &= 1 + 2.4699\,\eta^{3/2} + 9.7682\,\eta^3 - 144.5786\,\eta^5 + 246.7832\,\eta^7. & (3.5) \end{aligned}$$

Equivalent hard sphere diameter

There exists several approaches to assign an equivalent hard sphere diameter to a simple fluid atom (or molecule). Experimentally, these can be based on various approaches, including second virial coefficients, equation of state data and molecular refractivities (i.e. polarizabilities). Theoretical routes include Boltzmann's approach and perturbation theory (which comes in slightly varying forms).

Ben-Amotz and Hersbach [19] present a nice overview of the many ways an effective hard sphere diameter can be obtained. Common to all is that this diameter is temperature dependent, that is $\sigma = \sigma(T)$, and sometimes slightly density dependent as well (e.g., *WCA*). $\sigma(T)$ is always a decreasing function of temperature. This stems from the fact that a higher temperature, the increased kinetic energy allows atoms to explore close distances.

Several prescriptions and fits are available for $\sigma(T)$, and differ upon which classes of fluids are studied (e.g., metals, molecular fluids, Lennard-Jones model fluids). For metals, Protopapas et al. [12] first introduced:

$$\sigma(T) = \sigma_m \frac{1 - B(T/T_m)^{1/2}}{1-B}; \qquad B = 0.112 \tag{3.6}$$

Where T_m denotes the melting temperature. Protopapas et al. [12] define σ_m, the diameter at the melting temperature, as follows. They assume that for all liquid metals at T_m, the packing fraction at the melting point is a constant equal to 0.472:

$$\eta_m = \frac{\pi}{6}\rho\sigma_m^3 = 0.472 \tag{3.7}$$

This fixes[1] the value of σ_m. Notably, $\sigma(T)$ is based just on the melting temperature and the melting density.

Hard sphere fluid viscosity

Given that the Stokes-Einstein relation

$$D_{HS} = \frac{kT}{c\pi\mu_{HS}\sigma} \tag{3.8}$$

links the diffusion to the viscosity, μ_{HS}, it comes as no surprise that the equivalent hard sphere diameter can also be used to predict the viscosity of a liquid based on the value of an equivalent hard sphere fluid. In equation 3.8 the constant c equals 3 for stick BC's and equals 2 for slip BC's.

Protopapas et al. [13] describe this in a second paper. The Enskog theory approximation for the hard sphere viscosity is

$$\mu_E = \frac{5}{16\sigma^2}\left(\frac{mkT}{\pi}\right)^{1/2} 4\eta\left[\frac{1}{4\eta g(\sigma)} + 0.8 + (0.7614)4\eta g(\sigma)\right] \tag{3.9}$$

$$\equiv \mu_0 4\eta\left[\frac{1}{4\eta g(\sigma)} + 0.8 + (0.7614)4\eta g(\sigma)\right] \tag{3.10}$$

As was the case for the self-diffusion, MD simulations have provided a correction factor to lead to an expression for the viscosity[2]

$$\mu_{HS}(\eta) = \mu_E(\eta) f_\mu(\eta) \tag{3.11}$$

$$f_\mu(\eta) = \frac{16\sigma^2}{5}\left(\frac{\pi}{mkT}\right)^{1/2} \frac{2kT}{\pi D_E f_D(\eta)} \frac{1}{4.285 - 0.4128\eta} \tag{3.12}$$

Alternatively, an entirely empirical $f_\mu(\eta)$ can be generated by fitting experimental values of μ/μ_E, as was done by Protopapas et al. [13].

[1] Putting equations 3.6 and 3.7 together gives $\sigma(T) = 1.288\times10^{-8}\rho_m^{-1/3}[1 - 0.112(T/T_m)^{1/2}]$, with ρ_m the number density in cm^{-3} at the melting point

[2] This specific form arises from a fit to the product $\mu_{HS}D_{HS}$, which varies far more slowly than either term. In particular, a good fit to the MD data of Alder et al. [14] is $2kT/\pi\mu_{HS}D_{HS} = 4.2852 - 0.4128\eta$, see reference [13]

Chapter 4

Equilibrium Liquid Metals Mixtures

Given that the metals are atomic fluids and given that the pure metals liquids are so-called simple liquids, it is not surprising that liquid mixtures (alloys) of metals are simple liquid mixtures. However, that statement does not imply that all metal mixtures are simply ideal solutions (they are not). Immiscibility, partial miscibility, compound formation, and non-ideality are well within the scope of mixtures of simple liquids.

Molecular simulation of mixtures

To simulate a binary mixture of metals A and B requires an extension of the EAM approach to metals. For mixtures of noble gases, simple pair-potentials such as the well-known two-parameter Lennard-Jones potential can be used, and the two parameters (ε and σ) used for the pure fluid are replaced by species dependent ones: ε_{AA}, ε_{BB} and ε_{AB}, and similarly for σ. If the pure fluid parameters, ε_{ii} and σ_{ii}, with $i = A, B$ are known, estimates for the parameters, ε_{AB} and σ_{AB} can either be simply stipulated or alternatively constructed from the pure species values by the application of a so-called "mixing rule". For noble gases one often uses:

$$\begin{aligned} \varepsilon_{AB} &= (\varepsilon_{AA}\varepsilon_{BB})^{1/2} \\ \sigma_{AB} &= (\sigma_{AA} + \sigma_{BB})/2 \end{aligned} \tag{4.1}$$

These mixing rules are referred to as the Lorenz-Berthelot rules. They reproduce the exact second virial coefficient of the binary mixture. In practice, when a specific mixture is the focus, the values of ε_{AB} and σ_{AB} are fitted to some mixture property.

For metal mixtures where EAM potentials are used, a similar approach is taken. Johnson, and co-workers have provided generalized EAM potentials for 16 metals and their mixtures. The pure metals considered by Zhou et al are Cu, Ag, Au, Ni, Pd, Pt, Al, Pb, Fe, Mo, Ta, W, Mg, Co, Ti, and Zr.

Perturbation theory for mixtures

Perturbation theory for mixtures requires two ingredients. First, of course, one needs the interatomic potential function for the mixture. This was already described in the previous subsection. Second, one needs a reference fluid for the mixture of interest. This reference fluid is the hard sphere mixture. Then for each species a hard sphere diameter is determined using the WCA criterion. The free energy of the N-component hard sphere mixture is obtained from an accurate equation of state due to Mansoori and Leland. The $N(N+1)/2$ distinct radial distribution functions for the hard sphere mixture are usually obtained from the Percus-Yevick approximation, and used in integrals to obtain the attractive part of the energy and pressure. Again, a strict mean field theory results when one sets $g_{ij}(r) = 1$ for all combinations of i and j.

van der Waals one-fluid theory

This is an example of conformal solution theory, an approach that maps the fluid mixture at density ρ and temperature T onto a pure fluid characterized by a size parameter σ_0 and energy parameter ε_0, at some corresponding density and temperature. The theory hinges on finding a mapping that works. Van der Waals one-fluid theory has been very successful in this respect. It defines the following size and energy parameters

$$\sigma_0 = \sum_i \sum_j x_i x_j \sigma_{ij} \tag{4.2}$$

$$\varepsilon_0 = \sigma_0^{-3} \sum_i \sum_j x_i x_j \varepsilon_{ij} \sigma_{ij}^3 \tag{4.3}$$

where x_i denotes the molefraction of species i, and the cross terms σ_{ij} and ε_{ij} obtained using the Lorentz-Berthelot rules. With these in hand one then approximates the $g_{ij}(r)$'s by that of the equivalent pure fluid. The actual approximation consists of

$$g_{ij}(r/\sigma_{ij}; \rho, T, \mathbf{x}) \approx g_0(r/\sigma_0; \rho\sigma_0^3, kT/\varepsilon_0) \tag{4.4}$$

where $\mathbf{x} \equiv (x_1, x_2, ..., x_{N-1})$ denotes the composition vector of the $N-$component mixture.

CF-DFT of mixtures

The extension of DFT from pure fluids to mixtures contains two aspects. The attractive contribution is straightforward, and simply requires mixed coefficients for the attractive part of the interaction potential. The treatment of the reference fluid, a hard sphere mixture, is challenging, but has been made straightforward by Rosenfeld who developed the so-called fundamental measure theory [6]. Thus, the CF-DFT of liquid mixtures is now as straightforward as that of pure fluids, and can be readily used to generate surface tensions as a function of composition.

Dynamical Properties of liquid metals

Two dynamical properties are required in the description of reactive wetting problems, namely viscosity and diffusion. The viscosity, η, is a scalar quantity (for liquid metals) that depends on temperature, density and composition (T,ρ, and $\mathbf{x}$), and is needed at the continuum level to describe the flow of liquids. To describe multicomponent mass transport requires many Maxwell-Stefan (MS) diffusion coefficients $\mathscr{D}_{ij}$ that are also functions of the state point, i.e., T,ρ, and $\mathbf{x}$.

In this section, and the appendices, we will address how the viscosity and the MS diffusivities can be obtained. We use *equilibrium* techniques, such as the Green Kubo relationships, to calculate Onsager coefficients and MS diffusivities. Such quantities apply to mass transport problems that involve the dynamic behavior of systems *close* to equilibrium. However, the conditions encountered in metal joining, where rapid heating takes place, and sudden contacts are formed (e.g., between hot liquid metals and cold solid substrates), may in fact constitute *large* deviations from equilibrium. Extending the linear-response approach to situations far from equilibrium is currently the only viable strategy available. At this point there exists no complete theoretical framework that could treat the the large deviations, although there is much work is this developing field. However, MD simulations can be used to make an assessment of the limitations of the linear-response regime. That is, within an MD simulation one can study the dynamical behavior of large gradients and large external fields (such as in field-driven nonequilibrium MD (NEMD)) [24] and directly compare the results with the linear-response approach.

The driving force for diffusion of species i is the spatial gradient of its chemical potential[1], i.e. $\nabla\mu_i$. The transport equation is,

$$-\beta\nabla\mu_i = \sum_{j=1,j\neq i}^{m} \frac{x_j(u_i - u_j)}{\mathscr{D}_{ij}} \tag{4.5}$$

where $\beta = 1/kT$ and k is Boltzmann's constant. The velocity of species i is denoted by u_i. We see that $1/\mathscr{D}_{ij}$ acts as a friction coefficient, describing the friction between species i and j. It is immediately clear that for multicomponent mixtures a large number of MS diffusivities $\mathscr{D}_{ij}(\mathbf{x})$ are required, as many as there are distinct pairings of components, i.e. $m(m-1)/2$. Note that $\mathscr{D}_{ij} = \mathscr{D}_{ji}$.

The MS diffusivities are convenient quantities as their values are independent of the reference frame. Experimentally, these quantities are difficult to obtain directly because chemical potential gradients can not be measured directly. In general, the diffusivities are needed as a function of composition, and thus a large data set is required to address mass transport problems. Obtaining diffusivities from molecular dynamics simulations is comparatively straightforward (see Appendix B.), although sometimes it can be costly in computer time. However, if one seeks to limit the brute force MD approach it is crucial to explore predictive methods for the MS diffusion coefficients. This we will address in the sections below, where we outline a strategy that mini-

[1]There are only $m-1$ independent chemical potential gradients, as they satisfy the Gibbs-Duhem relationship.

mizes the amount of MD simulation to the simpler problem of determining self diffusion constants in multi-component mixtures.

Mutual Diffusion Coefficients of liquid metals mixtures. Enskog Theory

Following the success of Enskog theory of transport coefficients of the pure hard sphere limit first presented in 1922 [25, 26], it took many decades before the extension to the binary and later multicomponent hard sphere fluid was attempted by Thorne and, in 1971, by Tham and Gubbins [26, 27]. Lopez de Haro et al. [28] subsequently derived explicit expressions for the transport coefficients of heat and matter, based on the so-called revised Enskog theory. Later, Erpenbeck performed MD simulations for an isotopic binary mixture, and provided an excellent review of the subtle underlying issues in 1986 [29].

At this point in time there does not appear to be a generalization available of the work of Protopapas et al [12] that was described earlier, for pure metals. In other words, there exists currently no mapping strategy of the mutual diffusion coefficients of a metal mixture onto an appropriate hard-sphere mixture. This would appear to be a worthwhile direction to explore therefore.

A metal mixture could be characterized by the equivalent hard sphere diameters $\sigma_i(T)$ of the pure metals. The cross interactions between species i and j involves an prescription for σ_{ij}. For an additive mixture we expect that $\sigma_{ij} \approx (\sigma_i + \sigma_j)/2$, c.f., equation 4.1. In that case the metal mixture can be mapped onto an additive hard-sphere mixture of equivalent density, and the existing Enskog predictions of Lopez de Haro [28] couid be used. If the mixture is nonadditive, one could consider a mapping onto a nonadditive hard-sphere mixture, i.e., $\sigma_{ij} = (1+\alpha)(\sigma_i + \sigma_j)/2$, with α positive (preferring like neighboring spheres) or negative(preferring unlike neighbors). This would require MD results and Enskog theory to be generalized to nonadditive hard-sphere mixtures. This is straightforward for MD, but might more involved for the revised Enskog theory.

Mutual Diffusion Coefficients of liquid metals mixtures

Recently Liu, Vlugt and Bardow (LVB)[7] have introduced a robust method for predicting $\mathscr{D}_{ij}$, from self-diffusivities, $D_{i,self}$. The predictive method consists of multicomponent Darken equation derived from linear response theory and Onsager's relations. The result is

$$\mathscr{D}_{ij}(\mathbf{x}) = \frac{D_{i,self}(\mathbf{x}) D_{j,self}(\mathbf{x})}{D_{mix}(\mathbf{x})} \tag{4.6}$$

with

$$D_{mix}(\mathbf{x}) \equiv \sum_{i=1}^{m} \frac{x_i}{D_{i,self}(\mathbf{x})} \tag{4.7}$$

Equation 4.6, together with 4.7, is referred to as the multicomponent Darken equation, as it generalizes the familiar Darken equation for binary mixtures[2].

Equation 4.6, requires the self-diffusion coefficients, $D_{i,self}(\mathbf{x})$, of all the components in a multicomponent system of composition $\mathbf{x}$. To avoid this effort LVB introduced the following approximation

$$D_{i,self}(\mathbf{x}) \approx \left(\sum_{j=1}^{m} \frac{x_j}{D_{i,self}^{x_j \to 1}} \right)^{-1} \tag{4.8}$$

where $D_{i,self}^{x_j \to 1}$ is the infinite-dilution self-diffusion coefficient of species i in a binary mixture of i and j. When $j = i$, $D_{i,self}^{x_j \to 1}$ becomes te pure component self-diffusion coefficient (note that the summation in equation 4.8 includes the term $j = i$.)

The multicomponent Darken equation combined with the approximation 4.8 is referred to as the *predictive Darken-LVB* equation.

The approach outlined above is not the only approximate approach in the literature. For instance, the Vignes-LBV equation[7] is also based on pure component data together with binary mixture data:

$$\mathscr{D}_{ij} = (D_{j,self}^{x_i \to 1})^{x_i} (D_{i,self}^{x_j \to 1})^{x_j} \prod_{k=1, k \neq i,j}^{N} \left(\frac{D_{i,self}^{x_k \to 1} D_{j,self}^{x_k \to 1}}{D_{k,self}^{x_k \to 1}} \right)^{x_k} \tag{4.9}$$

Here $D_{i,self}^{x_j \to 1}$ is the infinite-dilution self-diffusion coefficient of species i in a binary mixture of i and j, while $D_{k,self}^{x_k \to 1}$ is the pure component self-diffusivity.

Viscosity of liquid metals mixtures

The viscosity of liquid mixtures, $\mu = \mu(T, \rho, \mathbf{x})$, is a scalar quantity that can be calculated using the Green-Kubo expressions, or alternatively from a *NEMD* simulation. Predictions based on the *pure* metals can be generated using a linear relation of the logarithm of the viscosity, as suggested by Arrhenius in 1887[15],

$$\ln\ \eta_{mix} = \sum_i x_i\ ln\ \eta_i \tag{4.10}$$

[2]For m=2, the multicomponent Darken equation reduces to the traditional Darken equation: $\mathscr{D}_{ij}(\mathbf{x}) = x_i D_{j,self}(\mathbf{x}) + x_j D_{i,self}(\mathbf{x})$

Grunberg and Nissan [16] suggested an extension of this expression to account for observed deviations

$$\ln\ \eta_{mix} = \sum_i x_i\ ln\ \eta_i + \sum_i \sum_j x_i x_j d_{ij} \tag{4.11}$$

where the constant d_{ij} can be positive or negative.

Eutectic mixtures

A eutectic system is a mixture (alloy) of a unique composition. It has a lower freezing point than any other composition of the same components. Thus, for the binary alloy of Sn and Pb, the freezing temperature is much below that of both the pure metals, see figure 4.1.

In our section on diffusion coefficients of liquid metals, we described the Darken-LVB prediction, which is based on the self diffusivities $D_{i,self}^{x_j \to 1}$ at the infinite-dilution self-diffusion coefficient of species i in a binary mixture of i and j at the same p and T. Its is clear that for a eutectic liquid mixture this approach breaks down in a serious fashion. This is because a mixture at infinite dilution and the *same* T might very well be a solid, or a combination of solid and a specific composition liquid mixture (of non infinite dilution character). Note that the equivalent hard sphere approach that was described in a previous section does not not suffer from this problem, as the temperature only enters through the description of the equivalent hard-sphere diameter $\sigma(T)$, and the hard sphere fluid phase diagram is only a function of density.

Although the eutectic mixture presents a problem for some approximate methods, such as the Darken-LVB prediction, the dynamic information (i.e., diffusivities and viscosity) can always be obtained from an MD simulation.

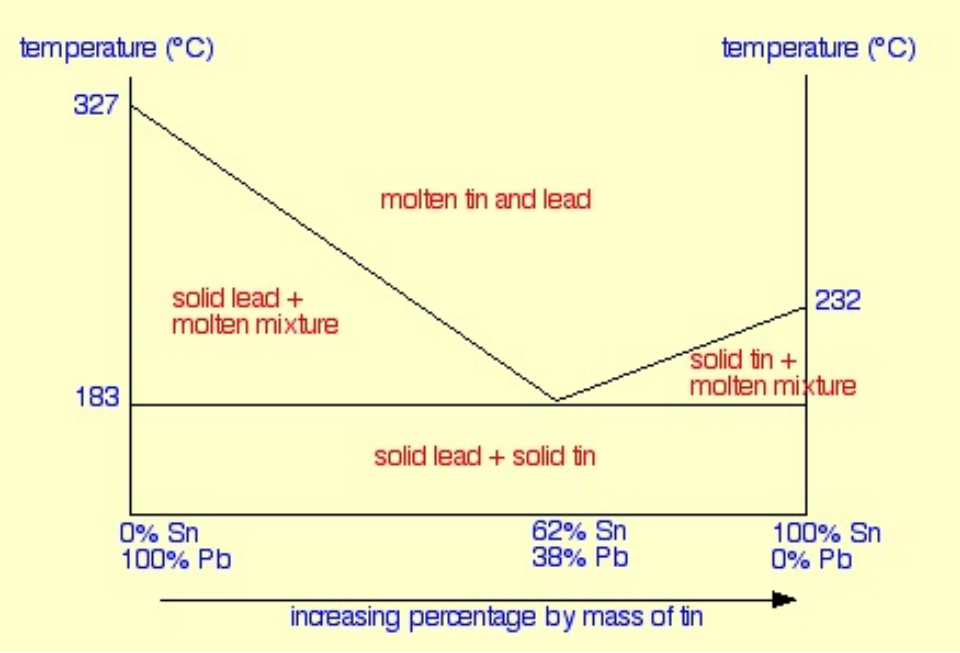

Figure 4.1. Schematic of the temperature composition diagram tin (Sn) lead (Pb) alloy. A eutectic occurs at 62 weight percent Sn. The melting temperature of pure lead is 327 °C, while pure tin melts at 232 °C. The eutectic freezing temperature is lower than both, and all other composition, i.e., 183 °C.

This page intentionally left blank.

Chapter 5

Recommendations

The molecular based phenomena discussed in this report and the analysis presented suggest a number of specific studies that would help to provide further insight into the phenomena that underlie active brazing process.

1. Surface segregation. Molecular dynamics, combined with Monte Carlo exchange moves, can be used to determine the degree of surface segregation. This should first be done for the two binary alloys of Ag with Cu, and Ag with Zr; varying the amount of the minority component (Cu or Zr) over the relevant range (roughly: $0-4\%$). Subsequently, the segregation should be investigated for the ternary Ag-Cu-Zr, over a similar range of compositions to determine if there are any cooperative effects present.

2. Surface melting. Molecular dynamics can be straightforwardly used to determine the presence or absence of surface melting, slowly heating a crystal at zero pressure. Naturally, one would first study this effect for pure Ag, considering the three low-index faces: (100), (110) and (111). The in-plane periodic boundary conditions require that we know the bulk lattice parameter as a function of temperature (T) and at zero pressure. This can be straightforwardly done with bulk NpT simulations, setting $p = 0$. Using the bulk lattice parameter as a function of T avoids any bulk stresses, and assures that the finite-sized simulation closely approximates the infinite system. Surface melting for alloys proceeds in an analogous way. Again, one requires the lattice parameter as a function of T at $p = 0$. As with the segregation studies, one would roughly cover the composition range $0-4\%$. In addition to the minor components Cu and Zr, which are of primary importance, one could also include the reaction product Al in this study.Finally, it would be very useful to consider experimental verification of surface melting. The challenge associated with such experiments are the high temperatures involved. This kind of study would be a first of its kind, as surface melting for mixtures has not been addressed in the literature.

3. Diffusion Coefficients. Molecular dynamics can be used to determine the self-diffusion coefficients of Cu and Zr in Ag. This can be done with standard NVT simulations, after determining the zero pressure density with NpT simulations. Using the theoretical approaches and approximations presented in this report one can then obtain values for the mutual diffusion coefficients.

4. Viscosity. The Green-Kubo analysis can be used to determine the viscosity coefficients from bulk NVT molecular dynamics simulations. As above, these results need to be

performed as a function of composition, and at constant pressure ($p = 0$).

The molecular simulation studies can be performed with an embedded atom potential (EAM). These interatomic potentials have been thoroughly tested for pure systems and mixtures and are known to produce reliable results. The surface melting study produce data as a function of T and composition. This data can be compared with predictions made solely based on the bulk phase diagrams. It is conceivable that some simple prediction might be developed for surface melting solely on the basis of bulk data and the amount segregation[1]. This would greatly facilitate the exploration of other potential brazes (i.e., different minority components).

The diffusion data can be used to determine a time-scale for the diffusion of the reactants and products which can be compared to the chemical kinetics of the surface reaction. The viscosity data can be used with the Washburn equation to predict the characteristic time-cale for the spreading of the liquid metal alloy. However, this requires information about the surface tensions (liquid-vapor and liquid-solid).

[1]It is also conceivable that a simple rule can be developed for the amount of segregation based on the surface energy of the pure metals. As described in the report and in ref [47] the energy of an impurity at the surface correlates well with the surface energy of the pure impurity metal

Chapter 6

Conclusion

In this report we have sought to address the broad question ”how can theory and molecular modeling help improve the active brazing joining process”. The report focuses various crucial aspects of the active brazing. For the commonly used braze, 97Ag-1Cu-2Zr, we have summarized the surface chemistry that leads to the conversion of Al_2O_3 and/or SiO_2 to ZrO_2. It is known that for a good bond between alumina and the braze, it is important to have this reaction occur. The creation of ZrO_2 at the interface directly improves the wetting and spreading of the molten braze. It is not known at this point, how much conversion is needed, let alone what would represent the optimal extent of reaction.

The current protocols have been arrived at primarily by trial and error. Simply performing the process under protocols that are ”known to work”, but without a thorough science-based understanding in place makes it very difficult to adjust to situations when ”every thing is done as usual” but the joints made are inferior or even fail. In addition, we note that the complexity of the process, and lack of understanding, makes quality control and quality assessments difficult.

Even if we did know the optimal composition of the interface in terms of the amounts of Al_2O_3, SiO_2 and ZrO_2, it would be challenging to accomplish that composition. This is because, the extent of the reaction is controlled by 1) the composition of the braze and 2) the heating and cooling cycle of the oven in which the brazing is done. The latter cycle is on a timescale of minutes to hours, and thus it is hard to use temperature to effectively quench a reaction, for example. If, on the other hand, surface melting is appreciable, it might be possible to just heat a temperature at which only the surface melts. This might allow one to accomplish the optimal extent of reaction, by limiting the amount of mobile reactant (Zr).

Molecular modeling could be of of significant help in providing a molecular level understanding of the coupled phenomena underlying brazing, and establishing the nature of dominant phenomena among the ones identified. Further, it could facilitate the exploration of alternative brazes (or alternative braze compositions), or the selection of more appropriate heating and cooling protocols in a more deliberate fashion.

The report has addressed several molecular phenomena, although not necessarily all. In particular, we highlight surface chemistry and surface melting. In addition we have included background information on the equilibrium behavior (e.g., thermodynamics and structure) of pure metals and alloys. The report discusses how to use self-diffusion coefficients (which are easy to calculate from a simulation) to provide information about mutual diffusion coefficients, as well as

the viscosity. Finally, the report mentions the composition effects on the nonequilibrium surface tension. This is a topic of much relevance in the general area of reactive wetting, and has been the focus of recent discussions and papers that address the challenge of continuum level-wetting simulation models.

References

[1] J.J. Stephens, F.M. Hosking, C.A. Walker, E.C. Dudley, F.G. Yost *The evolution of a ternary Ag-Cu-Zr active braze filler metal for kovar/alumina braze joints*, Proceedings of the 3rd international brazing and soldering conference, 2006, San Antonio Texas.

[2] E. Moret and N. Eustathopoulos, *Ceramic to metal direct brazing*, Journal De Physique IV Colloque C7, supplement au Journal de Physique 111, Volume 3, novembre 1993

[3] E. A. Carter and E. A Jarvis, *The role of reactive elements in thermal barrier coatings*, Computing in Science & Engineering March-April 2002 pg. 33.

[4] Equilibrium Software HSC Chemistry, see http://www.outotec.com/en/Products–services/HSC-Chemistry/

[5] J-M Zhang, B. Wang and K-W Xu, *Surface segregation of the metal impurity to the (100) surface of fcc metals*, Ind. Acad. Sci. **69**, 603 - 616 (2007)

[6] Y. Rosenfeld, Phys. Rev. Lett., **63**, 980 (1989)

[7] X. Liu, T.J.H. Vlugt and A. Bardow, Ind. Eng. Chem. Res., **50**, 10350 - 10358 (2011)

[8] Y.D. Shikhmurazev, *The moving contact line of a smooth solid surface.*, Int. J. Multiphase Flow., **19**, 589-610 (1993)

[9] T.D. Blake, *Dynamic contact angles and wetting kinetics*, Wettability, Ed. J.C. Berg, Marcel Dekker, New York, 251-309 ,(1993)

[10] T.D. Blake, M. Bracke, and .D. Shikhmurazev *DExperimental evidence of nonlocal hydrodynamic influence on the dynamic contact angle*, Phys. Fluids., **11**, 1995-2007 (1999)

[11] L. Mondy and many others, *Wetting and free surface flow modeling for potting and encapsulation*, Sandia report, SAND2007-3316, Albuquerque, New Mexico,(2007)

[12] P. Protopapas, H.C. Andersen, and N.A.D. Parlee, *Theory of transport in liquid metals. I. Calculation of self-diffusion coefficients.*, J. Chem. Phys., **59**, 15-25 (1973)

[13] P. Protopapas, H.C. Andersen, and N.A.D. Parlee, *Theory of transport in liquid metals. II. Calculation of shear viscosity coefficients.*, Chem. Phys., **8**, 17-26 (1975)

[14] B.J. Alder, D.M. Gass, and T.E. Wainwright, *Studies in Molecular Dynamics. VIII. The Transport Coefficients for a Hard-Sphere Fluid.*, J. Chem. Phys., **59**, 15-25 (1973)

[15] Arrhenius, Z. Physik. Chem., **1**, 285(1887)

[16] L. Grunberg and A.H. Nissan, *Mixture Law for Viscosity*, Nature., **164**, 799-800(1949)

[17] D. Ben-Amotz and D.R. Herschbach, *Estimation of Effective Diameters for Molecular Fluids.*, J. Phys. Chem., **94**, 1038-1047 (1973)

[18] R. Krishna and J.M. van Baten, *The Darken Relation for Multicomponent Diffusion in Liquid Mixtures of Linear Alkanes: An investigation using Molecular Dynamics (MD) Simulations.*, Ind. Eng. Chem. Res., **44**, 6939-6947 (2005)

[19] D. Ben-Amotz and D.R. Herschbach, *Estimation of Effective Diameters for Molecular Fluids.*, J. Phys. Chem., **94**, 1038-1047 (1973)

[20] X. Liu, A Martin-Calvo, E. McGarrity, S.K. Schnell, S. Calero, J-M. Simon, D. Bedeaux, S. Kjelstrup, A. Bardow and T.J.H. Vlugt, *Fick Diffusion Coefficients in Ternary Liquid Systems from Molecular Dynamics Simulations.* Ind. Eng. Chem. Res., **51**, 10247-10258 (2012)

[21] D.R. Wheeler and J. Newman *Molecular Dynamics Simulations of Multicomponent Diffusion 1. Equilibrium Method.*, J. Phys. Chem. B, **108**, 18353-18361 (2004)

[22] D.R. Wheeler and J. Newman *Molecular Dynamics Simulations of Multicomponent Diffusion 2. Nonequilibrium Method.*, J. Phys. Chem. B, **108**, 18362-18367 (2004)

[23] R. Taylor and R. Krishna *Multicomponent mass transfer* 1st ed.; *Wiley*: New York, NY (1993)

[24] D.J. Evans and G.P. Morriss *Statistical Mechanics of Nonequilibrium Liquids*, *Academic Press*: London, UK (1990)

[25] D.K. Enskog, *Svenska Vetenskapsaded. Handl*, 63, 4 (1922)

[26] S. Chapman and T.G. Cowling,*The Mathematical Theory of Nonuniform Gases*, 2nd ed. *Cambridge University Press* (1922)

[27] M.K. Tham and K.E. Gubbins *Kinetic Theory of Multicomponent Dense Fluid Mixtures of Rigid Spheres.*, J. Chem. Phys., **55**, 268-279 (1971)

[28] Lopez de Haro, E.G.D. Cohen and J.M. Kincaid *Kinetic Theory of Multicomponent Dense Fluid Mixtures of Rigid Spheres.*, J. Chem. Phys., **78**, 2746 (1983), and J. Chem. Phys., **79**, 4509 (1983)

[29] J.J. Erpenbeck *Transport coefficients of hard-sphere mixtures: Theory and Monte Carlo molecular dynamics calculations for an isotopic mixture.*, Phys. Rev. A., **39**, 4718-4731 (1989)

[30] C.F. Brooks, A.M. Grillet and J.A. Emerson *Experimental Investigation of Spontaneous Wetting of Polymers and Polymer Blends.*, Langmuir, **22**, 9928-9941 (2006)

[31] B.K. Yen, *X-ray diffraction study of mechanochemical synthesis and formation mechanism of zirconium carbide and zirconium silicides*, Journal of alloys and compounds **268**, 266-269 (1998) .

[32] S. Q. Wang and J. W. Mayer, *Reactions of Zr thin films with SiO_2 substrates*, J. Appl. Phys. **64**, 4711 (1988).

[33] S. Roberts and P.J. Dobson, *Evidence for reaction at the Al-SiO_2 interface*, J. Phys. D: Appl. Phys. **14** L17 (1981).

[34] J.J. Stephens, P.T. Vianco, P.F. Hlava, and C.A. Walker, *Microstructure and performance of Kovar Alumina Joints made with silver-copper active metal braze alloys*, Conference paper SAND99-1577C.

[35] R. E. Loehman and A. P. Tomsia, *Reaction of Ti and Zr with AlN and Al2O3*, Acta metal. mater. Vol. **40**, Suppl., S75 - S83 (1992).

[36] D. H. Kang, I-H Jung, *Critical thermodynamic evaluation and optimization of the AgZr, CuZr and AgCuZr systems and its applications to amorphous CuZrAg alloys*, Intermetallics **18**, 815 - 833 (2010).

[37] R. E. Loehman, B. D. Gauntt, F. M. Hosking, P. G. Kotula, S. Rhodes, J. J. Stephens, *Reaction and bonding of Hf and Zr containing alloys to alumina and silica*, Journal of the European Ceramic Society **23**, 2805 - 2811 (2003).

[38] R. E. Loehman, F. M. Hosking, B. Gauntt, P. G. Kotula, P. Lu, *Reactions of Hf-Ag and Zr-Ag alloys with Al_2O_3 at elevated temperatures*, J. Matls. Sci. **40**, 2319-2324 (2005).

[39] T.C. Shields and J.S. Abell, *Thick films of YBCO on alumina substrates with zirconia barrier layers*, Supercond. Sci. Technol. **5**, 627433 (1992).

[40] A. Christensen and E. A. Carter, *First-principles characterization of a heteroceramic interface: ZrO_2 (001) deposited on an α-Al_2O_3 (1102) substrate*, Physical Review B **62**, 16968 (2000).

[41] R. N. Patil and E.C. Subbarao, *Monoclinic-Tetragonal Phase Transition in Zirconia: Mechanism, Pretransformation and Coexistence*.Acta Cryst. **A26**, 535 (1970) .

[42] T-S Kim, K-H Kim, Takashi Goto and Byong-Taek Lee, *Microstructure Control of Al_2O_3/ZrO_2 Composite by Fibrous Monolithic Process*, Materials Transactions, **45**, No. 2 (2004) pp. 431-434.

[43] V. V. Srdic, S. Rakic, Z. Cvejic, *Aluminum doped zirconia nanopowders: Wet-chemical synthesis and structural analysis by Rietveld refinement*, Materials Research Bulletin **43**, 2727-2735 (2008).

[44] G. Baldinozzi, D. Simeone, D. Gosset, and M. Dutheil, *Neutron Diffraction Study of the Size-Induced Tetragonal to Monoclinic Phase Transition in Zirconia Nanocrystals*, Physical Review Letters **90** 216103-1 (2003)

[45] A. S. Barnard, Rakesh R. Y. and H. Xu, *Modelling the effect of particle shape on the phase stability of ZrO_2 nanoparticles*, Nanotechnology **17**, 3039 (2006)

[46] A. Suresh, M. J. Mayo, W. D. Porter and C. J. Rawn, *Crystallite and Grain-Size-Dependent Phase Transformations in Yttria-Doped Zirconia*, J. Am. Ceram. Soc., **86** 360-62 (2003).

[47] Y. Teraoka, M. Komaki, *Surface segregation and surface melting in segregating alloys*, Surf. Sci. **439** 1-13 (1999).

[48] Y. Teraoka, *A theoretical study of melting*, Surf. Sci., **281**, 317-322 (1993), and *Surface melting and superheating*, Surf. Sci., **294**, 273-283 (1993).

[49] Landolt-Bernstein New Series IV/5

Appendix A

Time Correlation Functions

A.1 On the calculation of time-correlation functions in hard sphere systems

In genereal, the viscosity can be written as a sum of three terms, involving kinetic ("K") and virial ("V") contributions, viz.,

$$\mu = \mu^{KK} + 2\mu^{KV} + \mu^{VV} \tag{A.1}$$

The Green-Kubo relation is

$$\mu^{AB}(\tau) = (kT)^{-1} \int_0^\tau dt c^{AB}(t) \tag{A.2}$$

where the correlation function is given in terms of the microscopic currents as

$$c^{AB}(t) = V^{-1} < J^A(0) J^B(t) > \tag{A.3}$$

here V denotes the volume. The two tensorial currents are

$$J^K = m \sum_i \mathbf{v}_i \mathbf{v}_i \tag{A.4}$$

$$J^V = -\frac{1}{2} \sum_{i \neq j} \mathbf{r}_{ij} \frac{\partial \phi(\mathbf{r}_{ij})}{\partial \mathbf{r}_{ij}} \tag{A.5}$$

$$\tag{A.6}$$

where $\mathbf{r}_{ij} = \mathbf{r}_i - \mathbf{r}_j$, and ϕ denotes the pair potential.

For hard spheres the force appearing in the current J^V is impulsive and hence the above expressions are not suitable for a simulation. In stead, one needs a formulation that is analogous to the mean square displacements used for diffusion.

A preliminary study of obtaining nonequilibrium tensions has been performed, and will be discussed elsewhere.

This page intentionally left blank.

Appendix B

Diffusion Coefficients

B.1 On the calculation of the diffusion coefficient

The self-diffusion coefficient can be obtained using a Green-Kubo (GK) expression involving a time integral of the velocity correlation function. For species i we have

$$D_{i,self} = \frac{1}{3}\int_0^\infty dt < \mathbf{v}_i(t)\cdot\mathbf{v}_i(t) > \tag{B.1}$$

where the angle brackets, $< \ldots >$, denote an average over all molecules of species i. Since the trajectory of a particle is the time integral of the velocity, i.e., $\mathbf{r}_i(t) = \mathbf{r}_i(0) + \int_0^t dt'\mathbf{v}_i(t')$ it follows that it is possible to rewrite this in terms of the mean squared displacements. Thus,

$$\begin{aligned} D_{i,self} &= \lim_{t\to\infty}\frac{1}{6t}[\mathbf{r}_i(t)-\mathbf{r}_i(0)]^2 & \text{(B.2)}\\ &= \lim_{t\to\infty}\frac{1}{6}\frac{d}{dt}[\mathbf{r}_i(t)-\mathbf{r}_i(0)]^2 & \text{(B.3)} \end{aligned}$$

This is referred to as the "Einstein" expression. Note that in a simulation with periodic boundary conditions (PBC) it is important that one does *not* simply use the current position in the MD box. To do so would always lead to a finite maximum displacement of order equal to the boxlength. Instead one must evaluate the displacement as $\mathbf{r}_i(t) - \mathbf{r}_i(0) = \int_0^t dt'\mathbf{v}_i(t')$, as the derivation suggests[1].

The Stefan-Maxwell equation (i.e., equation 4.5) given previously [7, 18, 20, 21, 22]

$$-\beta\nabla\mu_i = \sum_{j=1,j\neq i}^{m}\frac{x_j(\mathbf{u}_i-\mathbf{u}_j)}{\mathscr{D}_{ij}} \tag{B.4}$$

[1] This is sometimes referred to as using "unfolded" positions. That is, at time $t = 0$ one selects the current position, $\mathbf{r}_i(t)$, inside the MD box; and at later times when a particle crosses the boundary, $\mathbf{r}_i(0)$ represents the position of the appropriate image particle

where $\mathbf{u}_i =< \mathbf{v}_i >$, the ensemble averaged velocity of species i. Now, the Gibbs-Duhem relationship connects the chemical potential gradients, that is,

$$\sum_{i=1}^{m} x_i \nabla \mu_i = 0 \tag{B.5}$$

This reduces by one the number of equations in (B.4) to $m-1$. Using the molar average velocity as a reference velocity,

$$\mathbf{u} = \sum_{i=1}^{m} x_i \mathbf{u}_i \tag{B.6}$$

We rewrite (B.4) to obtain the $(m-1)$-dimensional matrix equation [18],

$$-\beta x_i \nabla \mu_i = \sum_{j=1}^{m-1} B_{ij} x_j (\mathbf{u}_j - \mathbf{u}). \tag{B.7}$$

The matrix $[B]$ can be expressed in terms of the diffusivities $\mathscr{D}_{ij}$. The off-diagonal, and diagonal elements are,

$$B_{ij} = -x_i \left(\frac{1}{\mathscr{D}_{ij}} - \frac{1}{\mathscr{D}_{iN}} \right); \qquad i, j(\neq i) = 1, 2, \ldots, m-1 \tag{B.8}$$

$$B_{ii} = \frac{x_i}{\mathscr{D}_{iN}} + \sum_{j \neq i}^{N} \frac{x_j}{\mathscr{D}_{ij}} \tag{B.9}$$

$$\tag{B.10}$$

repectively.

The Onsager coefficients, L_{ij}, are defined by (see Krishna and van Baten [18])

$$x_i \mathbf{u}_i = \beta \sum_{j=1}^{m} L_{ij} \nabla \mu_j; \qquad i = 1, \ldots, m \tag{B.11}$$

and correspond to a reference frame in which the mass-averaged mixture velocity is zero. That is, $\sum_i^m y_i \mathbf{u}_i = 0$, where y_i denotes the mass–fraction of species i. This implies that the Onsager coefficients satisfy

$$\sum_{i}^{m} M_i L_{ij} = 0 \tag{B.12}$$

where the molar mass of species i is denoted by M_i. The Onsager reciprocal relations require that the coefficients are symmetric, i.e., $L_{ij} = L_{ji}$.

Next, consider the inverse of the $(m-1)$-dimensional matrix [B],

$$[M] = [B]^{-1} \tag{B.13}$$

The matrix elements of $[M]$ are expressed in terms of the Onsager coefficients, L_{ij}, as [18]

$$M_{ij} = (1-x_i)\left(\frac{L_{ij}}{x_j} - \frac{L_{im}}{x_m}\right) - x_i \sum_{k=1\neq i}^{k=m} \left(\frac{L_{kj}}{x_j} - \frac{L_{km}}{x_m}\right); \qquad i,j = 1,2,\ldots,m-1 \tag{B.14}$$

$$\tag{B.15}$$

The Onsager coefficients can be calculated from an MD simulations using a GK expression,

$$L_{ij} = \frac{N_i N_j}{3N} \int_0^\infty dt < \mathbf{u}_i(t) \cdot \mathbf{u}_j(0) > \tag{B.16}$$

where N is the total number of molecules in the system ($N = \sum_i N_i$) and N_i denotes the number of molecules of species i.

Alternatively, one can apply an Einstein expression

$$L_{ij} = \lim_{t\to\infty} \frac{1}{6N} \frac{d}{dt} < [\mathbf{R}_i(t) - \mathbf{R}_i(0)] \cdot [\mathbf{R}_j(t) - \mathbf{R}_j(0)] > \tag{B.17}$$

where $\mathbf{R}_i/N_i = (1/N_i)\sum_{k\in i} \mathbf{r}_k$ denotes the center of mass position of species i. As pointed out, it is important that an MD implementation of equation B.17 uses the "unfolded" positions i.e. $\mathbf{r}_k(t) = \int_0^t dt' \mathbf{v}_k(t')$.

The expressions are much simplified for a binary mixture, $m = 2$, as the matrices $[B]$ and its inverse $[M]$ reduce to scalar quantities. We find that,

$$\begin{aligned} \mathscr{D}_{12} = M_{12} &= x_2\left(\frac{L_{11}}{x_1} - \frac{L_{12}}{x_2}\right) - x_1\left(\frac{L_{21}}{x_1} - \frac{L_{22}}{x_2}\right) \\ &= \frac{x_2}{x_1}L_{11} + \frac{x_1}{x_2}L_{22} - L_{12} - L_{21} \end{aligned} \tag{B.18}$$

The derivation of the GK expressions and the Onsager relationships originates with linear-response theory which describes the behavior of systems close to equilibrium, where external perturbations to the system are small compared to the natural thermal fluctuations. A thorough introduction into this area is provided by Evans and Morriss [24]. Those authors also describe the connection between homogeneous nonequilibrium strategies and the GK expressions.

B.2 Fickian Diffusivities

An alternative to the MS approach is based on a generalized Fick's law. In a molar reference frame[2] the generalized Fick's law for an $m-$component mixtures is given in terms of the mole-fraction gradients, ∇x_j, as

$$J_i = -c_t \sum_{j=1}^{m-1} D_{ij} \nabla x_j \tag{B.19}$$

Here J_i is the diffusion flux, c_t is the total molar concentration, and D_{ij} is the Fick diffusivity(to be distinguished from the MS diffusivity $\mathscr{D}_{ij}$). The D_{ij} are not symmetric, and their values are unrelated to their binary equivalents.

Given that the generalized Fick approach and the MS description consider the same physical transport process, D_{ij} must be related to $\mathscr{D}_{ij}$. In the same molar reference frame the relation is made through the matrix $[B]$ of equation B.10

$$[D] = [B]^{-1}[\Gamma] \tag{B.20}$$

where $[\Gamma]$ constitutes the matrix of thermodynamic factors

$$\Gamma_{ij} = \delta_{ij} + x_i \left(\frac{\partial ln \gamma_i}{\partial x_j} \right)_{p,T,\Sigma} \tag{B.21}$$

here δ_{ij} is the Kronecker delta, and the activity of species i is denoted by γ_i.

The constraint derivative is performed at constant pressure and temperature. The symbol Σ indicates that as x_j is varied all the other molefractions, except x_m, are kept constant, such that $\sum_{i=1}^{m} x_i = 1$ during the differentiation[3] It is clear that the presence of the thermodynamic factors in practice create a significant barrier. Experiments produce large uncertainties in γ_i and thus some Gibbs energy model is required to produce the desired information.

[2] Transformations into other reference frames can easily be made [23].

[3] The constrained derivative can be expressed in terms of a difference between two unconstrained derivatives [23]: .

$$\left(\frac{\partial ln \gamma_i}{\partial x_j} \right)_{p,T,\Sigma} = \left(\frac{\partial ln \gamma_i}{\partial x_j} \right)_{p,T,i \neq j} - \left(\frac{\partial ln \gamma_i}{\partial x_m} \right)_{p,T,i \neq m}.$$

Index

DISTRIBUTION:

1	MS 0836	Jermy B. Lechman, 1516
1	MS 0836	Richard C. Givler, 1513
1	MS 0840	Daniel J. Rader, 1513
1	MS 0878	R. Allen Roach, 2735
1	MS 1349	James E. Miller, 1815
1	MS 1411	Frank B. van Swol, 1814
1	MS 1411	A. C-T Sun, 1814
1	MS 0899	Technical Library, 9536 (electronic copy)

Sandia National Laboratories